Cross-conjugation and quantum interference

Valkenier, Hennie; Guedon, Constant M.; Markussen, Troels; Thygesen, Kristian S.; van der Molen, Sense J.; Hummelen, Jan C.

Published in:
Physical Chemistry Chemical Physics

DOI:
10.1039/c3cp53866d

Publication date:
2014

PCCP

PERSPECTIVE

View Article Online
View Journal | View Issue

Cite this: *Phys. Chem. Chem. Phys.*, 2014, **16**, 653

Cross-conjugation and quantum interference: a general correlation?†

Hennie Valkenier,‡[a] Constant M. Guédon,[b] Troels Markussen,[c] Kristian S. Thygesen,[c] Sense J. van der Molen*[b] and Jan C. Hummelen*[a]

We discuss the relationship between the π-conjugation pattern, molecular length, and charge transport properties of molecular wires, both from an experimental and a theoretical viewpoint. Specifically, we focus on the role of quantum interference in the conductance properties of cross-conjugated molecules. For this, we compare experiments on two series of dithiolated wires. The first set we synthesized consists of three dithiolated oligo(phenylene ethynylene) (OPE) benchmark compounds with increasing length. The second series synthesized comprises three molecules with different π-conjugation patterns, but identical lengths, *i.e.* an anthracene (linear conjugation), an anthraquinone (cross-conjugation), and a dihydroanthracene (broken conjugation) derivative. To benchmark reliable trends, conductance experiments on these series have been performed by various techniques. Here, we compare data obtained by conductive-probe atomic force microscopy (CP-AFM) for self-assembled monolayers (SAMs) with single-molecule break junction and multi-molecule EGaIn data from other groups. For the benchmark OPE-series, we consistently find an exponential decay of the conductance with molecular length characterized by $\beta = 0.37 \pm 0.03$ Å^{-1} (CP-AFM). Remarkably, for the second series, we do not only find that the linearly conjugated anthracene-containing wire is the most conductive, but also that the cross-conjugated anthraquinone-containing wire is less conductive than the broken-conjugated derivative. We attribute the low conductance values for the cross-conjugated species to quantum interference effects. Moreover, by theoretical modeling, we show that destructive quantum interference is a robust feature for cross-conjugated structures and that the energy at which complete destructive interference occurs can be tuned by the choice of side group. The latter provides an outlook for future devices in this fascinating field connecting chemistry and physics.

Received 11th September 2013,
Accepted 1st November 2013

DOI: 10.1039/c3cp53866d

www.rsc.org/pccp

Introduction

This perspective article focuses on the question of how the charge transport properties of molecular wires depend on their length and π-conjugation pattern. Most common molecular wires studied in molecular electronics, like oligophenylenes, oligo(phenylene ethynylene)s (OPEs) and oligo(phenylenevinylenes) (OPVs), are linearly conjugated, as defined by a strictly alternating sequence of single and double/triple bonds between the two ends of the wires. A second essential class of molecular wires features cross-conjugation. A pathway in a π-conjugated molecule is cross-conjugated if it contains two subsequent single bonds and the (sp^2 hybridized) carbon atom linking these single bonds is double-bonded to any group or atom in a third direction.[1] It has been known for decades that cross-conjugated groups show weaker electronic communication,[2] than linearly conjugated groups.[3–5] However, only recently has it become clear that destructive quantum interference (QI) effects play a key role in charge transport through cross-conjugated molecules.[6] According to calculations, quantum interference behavior in cross-conjugated molecules gives rise to a sharp drop in the transmission probability of electrons that have an energy between the HOMO (highest occupied molecular orbital) and LUMO (lowest unoccupied molecular orbital) levels.[4,7–10] This has drastic consequences for the conductance of molecular junctions. Furthermore, these and other QI effects[11–14] can be influenced by molecular structure and gating (in a three-terminal device), opening new

[a] *Stratingh Institute for Chemistry and Zernike Institute for Advanced Materials, University of Groningen, Nijenborgh 4, 9747 AG Groningen, The Netherlands. E-mail: J.C.Hummelen@rug.nl*
[b] *Kamerlingh Onnes Laboratorium, Leiden University, Niels Bohrweg 2, 2333 CA Leiden, The Netherlands. E-mail: Molen@physics.leidenuniv.nl*
[c] *Department of Physics, Center for Atomic-scale Materials Design, Technical University of Denmark, DK-2800 Kgs. Lyngby, Denmark*

† Electronic supplementary information (ESI) available: Synthesis procedures and characterization of compounds **AQ-A**, **AH-A**, **AH-B**, and **3**, details of the peparation of SAMs and analysis by XPS and ellipsometry, experimental details of the CP-AFM measurements, details of transport calculations, calculated energy levels, and additional transport calculations on AH. See DOI: 10.1039/c3cp53866d

‡ Present address: School of Chemistry, University of Bristol, Cantock's Close, Bristol BS8 1TS, UK.

routes to functional molecular devices such as switches,[15] memory devices,[16] transistors,[17–19] rectifiers,[20] and logic gates.[21]

Several conductance experiments comparing cross-conjugated and linearly conjugated molecules have been reported by now. To name a key set of results: much lower conductance values have been found for molecules with *meta*-substituted benzene rings as compared to *para*-substituted rings,[22–27] in agreement with calculations.[28] However, these systems have the disadvantage that not only the conjugation pattern of the molecular species measured is different; also their length and shape vary. Similar examples are found in molecular switches.[29] For instance, the core of diarylethene switches is linearly conjugated in the closed state, whereas it can be reversibly switched to the cross-conjugated open state upon irradiation.[30] Conductance switching between the more conducting closed and the less conducting open state of these optical switches has indeed been observed in various types of junctions.[31–37] Nevertheless, also for these switchable molecules, it is not just the conjugation pattern that changes: the geometry of these molecules and the framework of σ-bonds change dramatically as well. Clearly, for well-defined studies of cross-conjugation *versus* linear conjugation, a minimal change in molecular length (conformation) is desirable. This can be achieved by choosing different functional side groups. We have recently presented experimental evidence for QI using this philosophy.[38–40] Moreover, this strategy opens the door to length-preserving molecular switches which are required for fast switching with minimal structural reorganization, based on reduction and oxidation of their functional side group.[41–48]

The goal of this paper is two-fold. The first is to present a study on the relationship among molecular (cross-) conjugation, QI effects and conductance, both experimentally and theoretically. For this, we start by describing the synthesis of three rigid molecular wires with identical lengths and two thiolate anchoring groups to connect the wires to the gold electrodes. We have varied only the π-conjugation pattern of these molecular wires, which are cross-conjugated, linearly conjugated, and broken conjugated, respectively (see Fig. 1b). In addition, we have synthesized a series of linearly conjugated OPEs of increasing length as benchmark molecules (Fig. 1a). Next, we used our robust protocol for the formation of self-assembled monolayers (SAMs) from these molecules.[49] After having met these preconditions, we will present charge transport studies on these molecules. This brings us to the second goal of this paper, *i.e.* to compare conductance experiments on the same series of molecules by very different techniques, thus testing for reproducibility between methods in molecular electronics. Indeed, data from conductive probe Atomic Force Microscopy (CP-AFM)[50] will be compared to the results from single molecule conductance (break junction) and multi-molecular (EGaIn) experiments on these same series of molecular wires. To interpret the results and to present an outlook to future possibilities, calculations will be presented, showing how cross-conjugation gives rise to QI effects, affecting the electrical conductance dramatically, and how QI can be controlled by using various functional side groups.

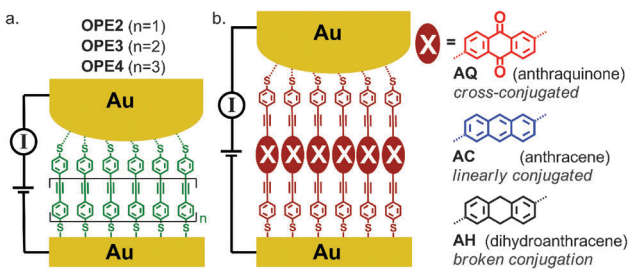

Fig. 1 Schematic of OPEs (a) and three molecular wires with different conjugation patterns (b) in the Conductive Probe Atomic Force Microscopy (CP-AFM) junction. A self-assembled monolayer of the molecular wires is grown on a gold coated silicon substrate and contacted with a gold coated AFM tip, after which the current through the junction is measured *vs.* bias voltage.

Results & discussion

Synthesis of the molecular wires

All molecular wires in this study have similar structural motifs and two thiol terminals, for self-assembly onto gold surfaces. We protected these thiols with acetyl groups, to obtain stable compounds that can be stored as solids in air and of which the protecting groups can be removed *in situ* during the formation of SAMs.[49,51] We described the synthesis of the OPE series in ref. 52. The synthesis of the wires **AQ**, **AC**, and **AH** with different π-conjugation patterns and identical lengths (24 Å[53]) follows the same strategy and is outlined in Scheme 1. First we synthesized the core units of the molecular wires, which determine their conjugation patterns. Cross-conjugated 2,6-dibromo-9,10-anthraquinone (**1**)[54] was reduced with sodium borohydrate to obtain linearly conjugated 2,6-dibromoanthracene (**2**) according to literature procedures.[55,56] The conjugation pattern of the third core unit (**3**) is broken by sp^3 hybridized carbon atoms 9 and 10. This 2,6-dibromo-9,10-dihydroanthracene[57] **3** was obtained by a reduction of 2,6-dibromo-9,10-anthraquinone with red phosphorus, iodine, and aqueous hydroiodic acid in a sealed ampule[58,59] in 58% yield, contaminated with 2-bromo-6-diodo-9,10-dihydroanthracene (~20%, this compound reacts in the next step in the same way as compound **3** does).

We synthesized the molecular wires in two steps: a Sonogashira cross-coupling of the dibromo-compounds with 1-*tert*-butylthio-4-ethynylbenzene (**4**) yielded the wires with *tert*-butyl protecting groups (-B), followed by an exchange of the *tert*-butyl protecting groups by the more labile acetyl groups (-A). The Sonogashira cross-coupling of **3** and 1-*tert*-butylthio-4-ethynylbenzene under the conditions as used for the syntheses of anthraquinone wire **AQ-B**[41] and anthracene wire **AC-B**[52] gave only 16% conversion to **AH-B**, due to deactivation of the C–Br bonds in **3** towards the oxidative insertion, caused by the two methylene groups on the phenyl rings.[60] Replacing the solvent system by pure triethylamine improved the conversion to **AH-B**, which was isolated in 25% yield.

The reactions of **AC-B** and **AH-B** with boron tribromide and acetyl chloride[61] yielded target molecular wires **AC-A**[52] and **AH-A**.

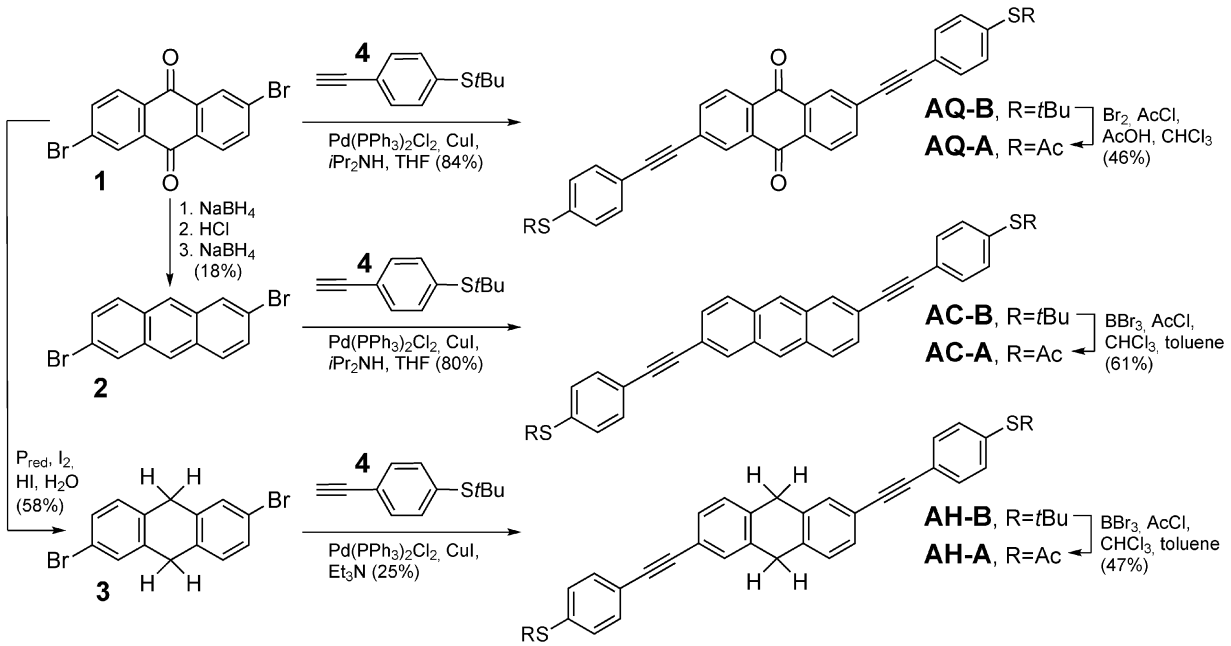

Scheme 1 Synthesis of the molecular wires **AQ**, **AC**, and **AH**, *via* Sonogashira cross-coupling reactions, followed by deprotection and acetylation of thiol terminals. Yields are given in parentheses.

Since boron tribromide was found to react with the anthraquinone core of **AQ-B**, this compound was treated with a trace amount of bromine[62] and reprotected with acetyl chloride, to obtain the cross-conjugated target anthraquinone-wire **AQ-A**.[63] Details of the syntheses and characterization of **AH-A** and **AQ-A** are reported in the ESI† and of **AC-A** in ref. 52.

UV-vis absorption spectroscopy

The UV-vis absorption spectra of the molecular wires were measured to gain information regarding their optoelectronic structure (Fig. 2). Whereas the absorption of **AQ** and **AC** exceeds 400 nm, the absorption of **AH** ends abruptly at 330 nm, resulting in an optical HOMO–LUMO gap of 3.75 eV. The broken conjugation of this molecular wire is reflected by its absorption: the molecule is effectively divided into two chromophores that have an absorption spectrum very similar to that of **OPE2**.

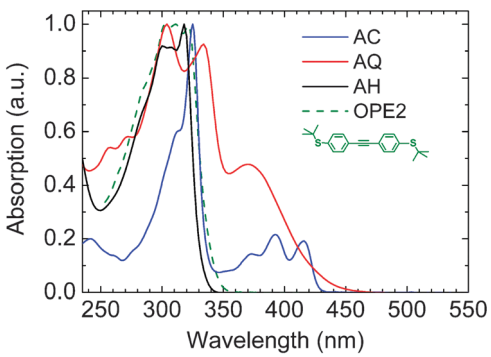

Fig. 2 UV-vis absorption spectra of 10^{-5} M solutions of **AQ** (red), **AC** (blue) and **AH** (black) in dichloromethane, which show a similar optical HOMO–LUMO gap for cross-conjugated **AQ** and linearly conjugated **AC**, whereas the spectrum of **AH** resembles that of **OPE2** (structure shown in green), reflecting the broken conjugation of **AH**.

Interestingly, the optical gaps of wires **AQ** and **AC** in dichloromethane are nearly identical (2.88 and 2.90 eV respectively). Even though the electronic communication in cross-conjugated compounds is in general lower than in linearly conjugated compounds, resulting in a larger HOMO–LUMO gap, the optoelectronic gap of cross-conjugated molecules that have both strong electron donating and accepting groups (*i.e.* in a push–pull configuration) is known to be smaller compared to cross-conjugated molecules without these groups.[3,64] The anthraquinone unit in **AQ** is a strong electron accepting group, which decreases its LUMO level significantly, whereas the thio-substituted phenyl ring can act as a donor, explaining the small optoelectronic HOMO–LUMO gap of wire **AQ**.[65]

This internal donor–acceptor character of **AQ** is also apparent in Fig. 3, which shows the molecular orbitals (MOs) of the free **AQ**, **AC**, and **AH** as obtained from DFT (density functional theory) calculations (see ESI† for details). The HOMO of **AQ** is mainly located at the thio-substituted phenyl rings (donor), whereas the LUMO is clearly located at the electron accepting anthraquinone unit. The very small energy difference between the HOMO and HOMO − 1 of **AH** in combination with their distribution (right part is mirrored where the left parts are identical) highlights the decoupling between the two parts of the conjugated system of **AH**.

Conductance measurements

Here, we first present conductance data for SAMs, obtained by conductive probe Atomic Force Microscopy (CP-AFM), for the two molecular series. Interestingly, the same sets of molecules, synthesized in the same lab (University of Groningen), have been

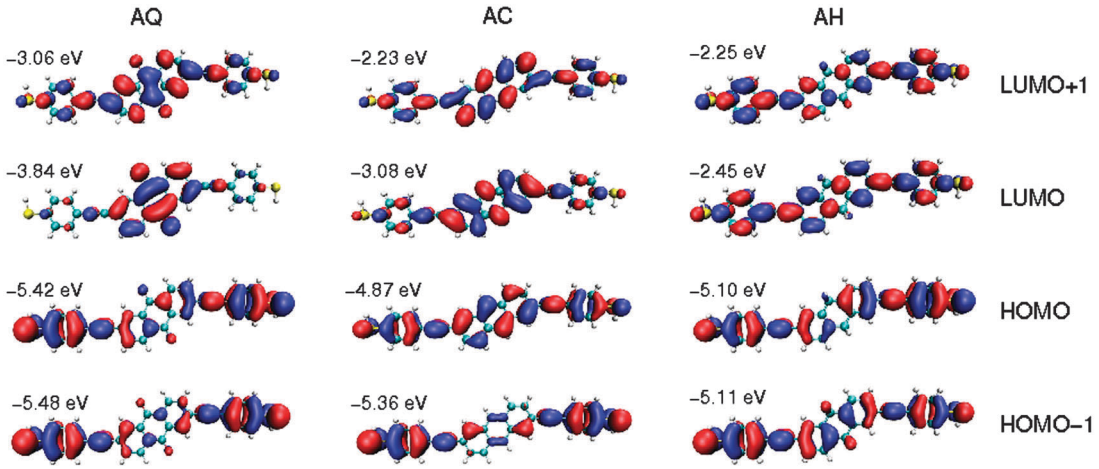

Fig. 3 Molecular orbitals (MOs) of free **AQ**, **AC**, and **AH**. The Kohn–Sham orbital energies for each MO is given relative to the vacuum level (see ESI† for details).

independently measured in two other groups, using different experimental methods. This gives us the unique opportunity to compare experimental results obtained by various techniques and to test for mutual consistency. First, the OPE series is used as a basic benchmark. Next, we focus on the data sets for **AC-AQ-AH**.

To perform our measurements, the molecules were connected to a bottom electrode by a well-defined self-assembly procedure. The bisacetyl-protected dithiols can spontaneously form self-assembled monolayers (SAMs) on gold. However, these SAMs are not densely packed.[49] Therefore we have added 10–13% triethylamine as a deprotecting agent to the 0.5 mM solutions of the wires **AQ**, **AC**, and **AH** in chloroform, as we did to the solutions of OPEs in THF.[49] We have immersed gold-covered substrates for two days in these solutions (under nitrogen). The resulting SAMs were analyzed by ellipsometry and X-ray photoelectron spectroscopy (XPS), which confirmed that monolayers of molecules that are oriented upright were present. These data are presented and discussed in the ESI.† We have contacted the SAMs of the molecular wires on gold-coated silicon samples with a gold-coated contact mode AFM tip (Fig. 1). The current through these junctions was measured as a function of the bias voltage. The low-bias conductance was obtained from a linear fit of the *I–V* curves at biases running from −100 mV to 100 mV. To obtain significant statistics, we measured about 200–1000 *I–V* curves per spot and 3–6 spots per sample, allowing us to construct the conductance histograms shown in Fig. 4a and c. Since the exact geometry of the contact and thus the number of molecules contacted varies from measurement to measurement, a spread in conductance values is found.[66]

The conductance histograms of the series **OPE2-OPE3-OPE4** (see Fig. 4a,) show that the conductance decreases strongly with the length of the OPE-type molecules. To find the most probable conductance values, we fitted the logarithm of the conductance values with Gaussian distributions. In Fig. 4b, we show a semi-logarithmic plot of these values *versus* the molecular length (blue diamonds). The data are quite well described by a relationship of exponential decay between the conductance G and molecular length L, in agreement with the empirical, tunneling-like relationship $G = G_i \cdot e^{-\beta L}$ (with G_i a prefactor). The slope of the plot quantifies the decay parameter β and we find $\beta = 0.37 \pm 0.03$ Å^{-1}.

Let us now compare these data to the single-molecule conductance values obtained by Wandlowski's group on the same molecular series. Specifically, they used both Mechanically Controllable Break Junctions (MCBJ) and Scanning Tunneling Microscopy Break Junctions (STM-BJ) to measure the OPE-series.[52] Fig. 4b makes the comparison, where the single-molecule values were all scaled up by an arbitrary factor of 100 to compensate for the larger number of molecules contacted in a CP-AFM junction.[67] There is rather good correspondence between the three data sets. The β values obtained from these single molecule studies are 0.34 ± 0.01 and 0.33 ± 0.02 Å^{-1}, respectively, which are very close to the values obtained from CP-AFM measurements. This demonstrates the robustness of measurements on this series of OPE molecules by different labs and in different types of gold-dithiolated molecule–gold junctions. We should note that some of us found a β value of only 0.07–0.15 Å^{-1} for this same series of OPEs when measured in large area molecular junctions with a bottom contact of gold and a top contact of the water soluble polymer PEDOT:PSS.[49] However, the interpretation of these data has turned out to be non-trivial, since in many cases, especially when conjugated molecules are studied, the top contact dominates the current–voltage characteristics.[68,69] In the literature, various β values for OPEs have been reported: 0.21 Å^{-1} by Liu *et al.* in CP-AFM junctions,[70] 0.32 Å^{-1} by Xing *et al.* in STM junctions,[71] 0.20 Å^{-1} for amine terminated OPEs by Lu *et al.* in STM junctions,[72] 0.33 Å^{-1} for acetylene terminated OPEs by Hong *et al.* in STM junctions,[73] and 0.36 Å^{-1} by Creager *et al.* in charge transfer experiments.[74] This scatter in literature values for one of the benchmark molecular series emphasizes the need for a comparison of techniques within one coordinated effort, as presented here.

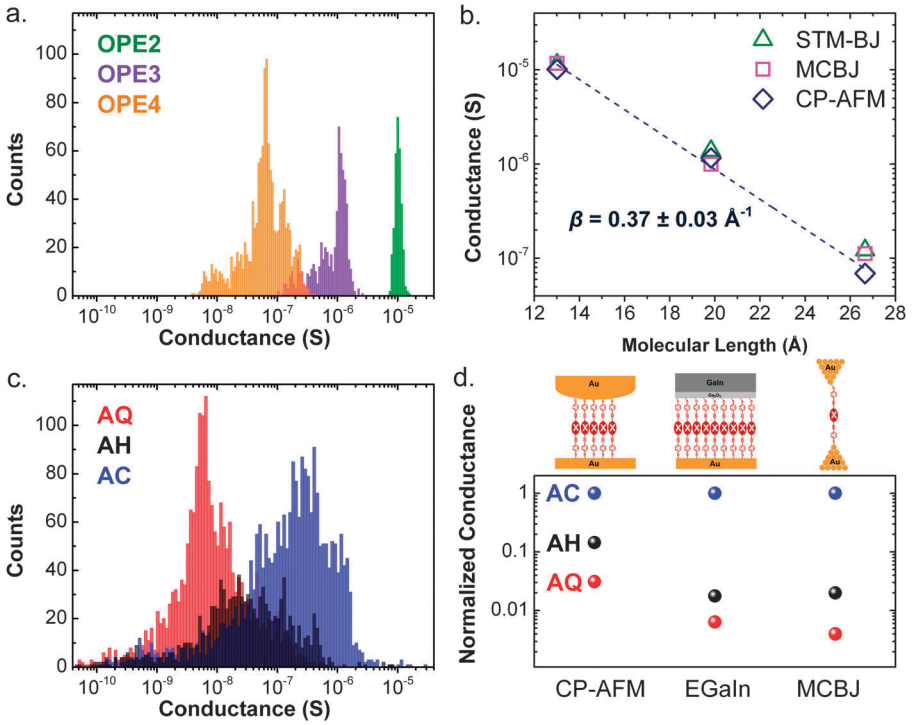

Fig. 4 Histograms of the low-bias conductance of (a) **OPE2** (green) **OPE3** (purple) and **OPE4** (orange) and (c) **AC** (blue), **AQ** (red), and **AH** (black) SAMs, measured by CP-AFM. (b) The conductance values of **OPE2–4** decrease exponentially with the length of the molecules, identical to the decrease found in MCBJ and STM-BJ (those conductance values are multiplied by 100 to compensate for the larger number of molecules contacted in CP-AFM junctions). (d) In the series of molecules with different conjugation patterns, linearly conjugated **AC** features the highest values, within statistical error and cross-conjugated **AQ** the lowest. This trend is the same in CP-AFM, EGaIn, and MCBJ junctions.

After having established reliable measurements on SAMs of OPEs, we studied the conductance of SAMs from the series of molecules **AC-AQ-AH**, with different π-conjugation patterns and identical lengths (Fig. 4c). Linearly conjugated **AC** clearly shows the largest conductance. A Gaussian fit of its histogram is centered at around 2×10^{-7} S. This conductance value is about two orders of magnitude larger than the conductance value of $2.5-3.5 \times 10^{-9}$ S found in single molecule conductance studies on **AC**,[40,52] again in agreement with our estimation that about 100 molecules are contacted on average in a CP-AFM junction (*cf.* our study of OPEs). For the cross-conjugated wire **AQ**, we measured conductance values (7×10^{-9} S) that are almost two orders of magnitude lower than for linear conjugated **AC**. Remarkably, compound **AH** gave conductance values of around 3×10^{-8} S, *i.e.* lower than **AC**, but higher than **AQ**, within statistical variation. To verify this trend, we again compare to single molecule MCBJ studies by Wandlowski's group.[40,52] In addition, we include recent studies on larger areas of SAMs of the same molecular series. These latter measurements were done using a tip of the eutectic alloy of gallium and indium (EGaIn) as a top contact to connect billions of molecules in parallel, by Chiechi and co-workers.[39] Fig. 4d makes the comparison, by normalizing the conductance of **AC** to 1 and plotting the conductance values of **AH** and **AQ** relative to **AC**. Indeed, all three methods show that the conductance of cross-conjugated **AQ** is about two orders of magnitude lower than the conductance of linearly conjugated **AC**. Moreover, the conductance of **AH** with its broken conjugation is found to be higher than that of **AQ** in all three data sets. This rather surprising order directly demonstrates that transport through a cross-conjugated junction does not depend trivially on the HOMO–LUMO gap and electron (de)localization alone. Indeed, another component is needed to explain the low conductance values found consistently for **AQ**. In the following sections we will discuss the observed trend in more detail and we discuss its relation with the energy levels of the molecules and QI phenomena.

Transport calculations

Since the trend in conductance of the molecular wires **AQ**, **AC**, and **AH** is not trivial from a chemistry perspective, we have calculated their charge transport properties with density functional theory (DFT)-based methods. Indeed, even though **AQ** has a considerably smaller HOMO–LUMO gap than **AH**, the conductance of **AQ** is lower. We relate this to a quantum interference effect in **AQ** which lowers the conductance significantly.[15,38] Fig. 5 shows the calculated transmission functions for **AQ** (red), **AC** (blue) and **AH** (black). These transmission functions, $T(E)$, give the probability that an electron with electron energy E tunnels from one side of the junction to the other. The transmission function of **AQ** shows a clear transmission dip at around $E - E_F = 0.7$ eV (where E_F is the Fermi energy) while no such dip is observed for **AC** or **AH** in the considered energy range.

The transmission functions in Fig. 5 were calculated using the DFT + Σ method.[75] While standard DFT in general overestimates

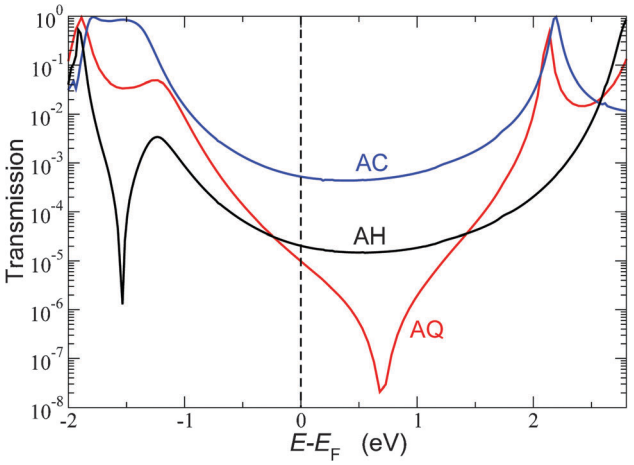

Fig. 5 Transmission functions $T(E)$ for **AQ** (red), **AC** (blue) and **AH** (black), as calculated by DFT + Σ.

the conductances, a simple correction of the levels has been found to improve agreement with experiments.[76,77] In this DFT + Σ method, the DFT Kohn–Sham gap ($\Delta\varepsilon_{HL}$) is corrected in the following way: first, the empty (occupied) states are shifted up (down) in energy by the amounts ε_L − EA (ε_H − IP). This ensures correct levels of the gas-phase molecule. Secondly, image charge corrections are included through a simple model[76,78,79] which shifts the empty (occupied) levels down (up) in energy. For the OPE-series we find an exponentially decreasing conductance *vs.* length for both DFT and DFT + Σ calculations with decay constants β_{DFT} = 0.16 Å^{-1} and $\beta_{DFT+\Sigma}$ = 0.31 Å^{-1}, respectively. Interestingly, while standard DFT calculations give a significantly different decay constant, the decay constant obtained from the energy level corrected DFT + Σ calculations is in good agreement with the experimental observations (see Fig. 4b).

In Table 1 we list the experimental zero bias conductances of **AQ**, **AC**, and **AH** together with values calculated from DFT and from DFT + Σ. The correction of DFT energy levels in the DFT + Σ approach does lead to quantitative changes, but the trends are the same: **AC** has the highest conductance while **AQ** has the lowest. We cannot directly compare the calculated single-molecule conductance values with the experimental values. Therefore we show in the last three columns in Table 1 the *relative* conductance differences between the three molecules. These numbers are independent of the number of molecules in the junction, assuming that the average number of molecules in contact with the AFM tip is also the same. The conductance ratios obtained with the DFT + Σ method indicate that **AC** has a 45 times larger conductance than **AQ**, while that of **AH** is two times larger than **AQ**. These ratios are in reasonable agreement with the experimental trends in Fig. 4d for all methods, and specifically for our CP-AFM study, where we find a much larger conductance for **AC** than for **AQ** (a factor of around 40), and a larger conductance for **AH** relative to **AQ** (a factor of around 5). We stress that the conductance of particularly **AQ** is sensitive to the exact position of the Fermi level, which is difficult to calculate accurately within DFT (and DFT + Σ). This can be seen from the relatively large slope of the **AQ** transmission at E_F which is caused by QI. A small change in the Fermi level of +0.1 eV with respect to the molecular levels could thus lead to a reduction of the **AQ** conductance by a factor of 2, while the **AH** and **AC** values hardly change.

Table 1 A comparison of experimental (see Fig. 4c and d) and calculated conductance values for the **AC**, **AH**, **AQ** series. G_{DFT} and $G_{DFT+\Sigma}$ are the low-bias conductance calculated with DFT and DFT + Σ, respectively

Molecular wire	G_{exp} (G_0)	G_{DFT} (G_0)	$G_{DFT+\Sigma}$ (G_0)	G_{exp}/G_{AC}	G_{DFT}/G_{AC}	$G_{DFT+\Sigma}/G_{AC}$
AC	3.2×10^{-3}	7.1×10^{-3}	5.0×10^{-4}	1	1	1
AH	4.0×10^{-4}	8.9×10^{-5}	2.0×10^{-5}	1/8	1/80	1/25
AQ	7.9×10^{-5}	4.6×10^{-5}	1.1×10^{-5}	1/40	1/150	1/45

The interference phenomenon can be qualitatively understood by transforming the frontier orbitals into localized molecular orbitals (LMOs). Since the HOMO − 1 and HOMO are almost degenerate, both are relevant for the transport in the HOMO–LUMO gap. The transformation of the HOMO − 1, HOMO, and LUMO into LMOs leads to a simple three-level tight-binding model where the electron can pass through the molecule in two ways, which interfere destructively in the HOMO–LUMO gap.[38] For **AC** the HOMO and LUMO are well separated in energy from the other MOs and it suffices to consider only these two orbitals. This leads to a two-level model with only a single path through the molecule and consequently no QI effects. A similar analysis for **AH** presented in the ESI† shows that the QI dip at $E - E_F$ = −1.5 eV is due to an interplay between the HOMO − 3 and HOMO states. Notice that both **AQ** and **AH** show reduced transmission peaks at around $E - E_F$ = −1.2 eV which do not approach unity. This is due to the quasi-degenerate HOMO and HOMO − 1 levels (see Fig. 3), which cause additional QI due to the different symmetry of the two states. This type of QI due to quasi-degenerate levels has recently been studied both theoretically[80] and experimentally.[11]

Controlling QI in cross-conjugated wires with different side groups

The conductance measurements show that cross-conjugated **AQ** has a lower conductance than linear conjugated **AC** and even than broken-conjugated **AH**. The question remains if this difference is caused solely by the cross-conjugation of **AQ** or if the strong electron accepting nature of the anthraquinone unit plays a role for the destructive QI. For that reason, and to provide an outlook to future experiments and devices, we have studied the transmission functions of several cross-conjugated analogue wires that have different energy levels (or electron donating/accepting character).

The origin of the QI in the cross-conjugated **AQ** is a p_z orbital of the oxygen side groups. According to relatively simple Hückel calculations,[81] the energetic position of the QI transmission dip can be tuned by varying the on-site energy of the side group p_z orbital. Electron accepting side groups will have an on-site energy $\varepsilon_{sg} < E_F$, while electron donating side groups will have $\varepsilon_{sg} > E_F$. By tuning the side group the position of the QI transmission node can consequently be controlled. For side group energies

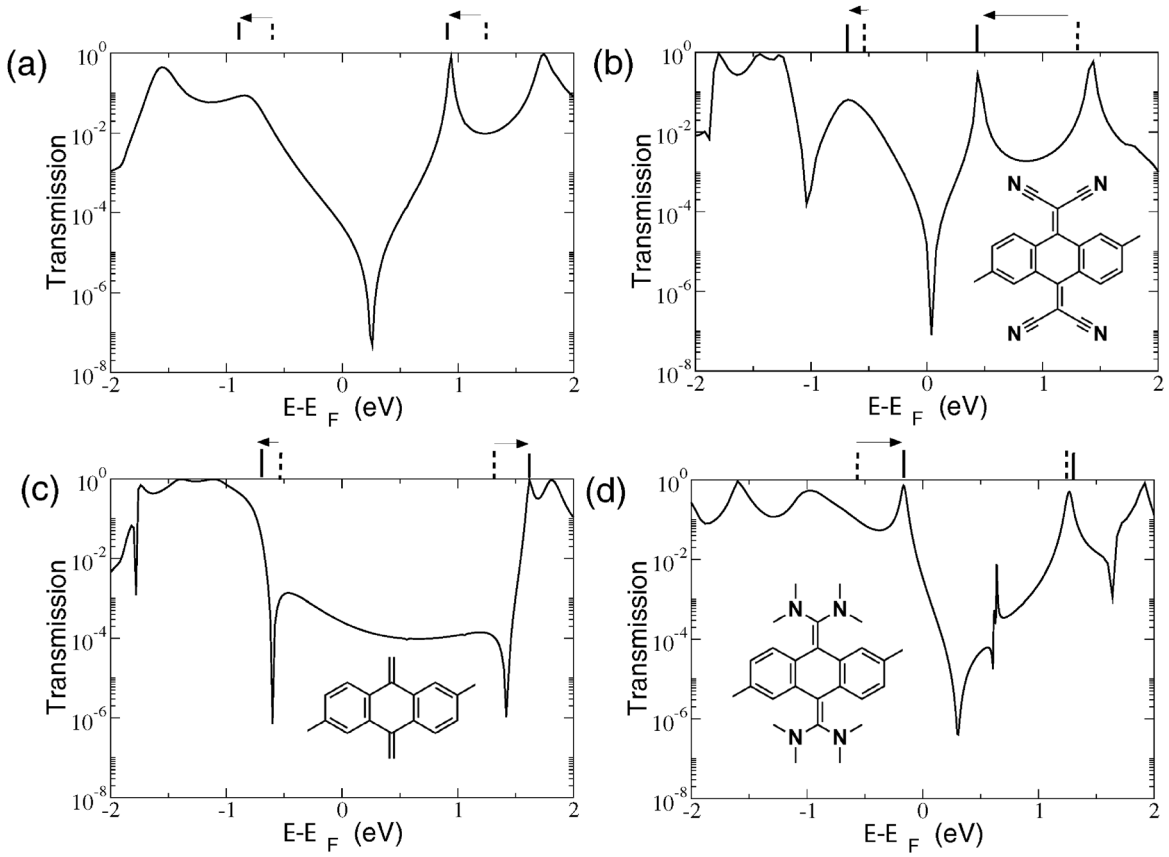

Fig. 6 DFT transmission functions for cross-conjugated **AQ**-like molecules with different side groups: (a) oxygen, (b) TCAQ, (c) CH_2, and (d) TDA. The vertical solid lines in the top parts mark the HOMO and LUMO of the molecules while the dashed lines indicate the HOMO and LUMO of **AC**. It is evident that the electron donating side groups O and $C(CN)_2$ push the levels down in energy whereas the electron withdrawing side group $C(NMe_2)_2$ pushes the HOMO level up in energy. The neutral CH_2 side group leads only to minor shifts due to hybridization effects.

relatively close to the Fermi energy, it is furthermore expected that there should be two QI transmission nodes in the HOMO–LUMO gap.[81]

Fig. 6 shows the transmission functions (calculated using DFT without any correction of energy levels) for four different AQ-like molecules with different side groups at the cross-conjugated site. The molecules in Fig. 6b and d are inspired by known redox active molecules tetracyanoquinodimethane (TCNQ) and tetrakis(dimethylamino)ethylene (TDAE) respectively. As for the anthraquinone containing wire in Fig. 6a, this would in principle allow for switching between this cross-conjugated state and a linearly conjugated state.[41] The insets show the central part of each molecule. Panels (a) and (b) show results for the electron withdrawing side groups O (**AQ**) and a 2,6-disubstituted tetracyanoanthraquinone-based structure (TCAQ), respectively. When comparing the HOMO and LUMO levels (marked by vertical solid lines in the top) to the HOMO and LUMO of **AC** (vertical dashed lines) it is evident that effect of the side group is to shift the whole electronic spectrum down in energy. This is expected due to the electron withdrawing nature of the side groups and is in agreement with previous studies.[20] In accordance with Hückel calculations,[81] two QI transmission dips are observed for TCAQ (b), with the lower QI minimum being located below the HOMO level. For **AQ** (a) additional minima are also observed but at even lower energies. The neutral CH_2 side groups (c) clearly induce two transmission nodes in the HOMO–LUMO gap and there is no overall shift of the energy levels. The electron donating tetrakis(dimethylamino) side group (TDA, d) shifts the HOMO level upwards in energy and also displays multiple QI transmission dips in the HOMO–LUMO gap. Due to steric repulsions the TDA side groups are rotated out of the anthracene plane and the coupling to the side groups becomes very small. This results in a side group orbital at energy $E - E_F = 0.6$ eV which is only weakly coupled to the main wire. This is the origin of the Fano-like shape in the transmission function at around $E - E_F = 0.6$ eV where a transmission dip is right next to a peak.

From the calculated transmissions for different side groups we conclude that (i) the energy spectrum can be shifted down or up relative to **AC** by using electron withdrawing or electron donating side groups, respectively. (ii) All cross-conjugated molecules have at least one QI transmission node in the HOMO–LUMO gap which is expected to strongly influence an experimentally measured conductance. (iii) The main trends for the transmission nodes are in agreement with simple Hückel calculations.

Interestingly, the ability to tune both the molecular levels and the QI transmission nodes is potentially promising for thermoelectric applications. Thermoelectric materials can be used to convert thermal energy into electrical energy in order to

e.g. harness waste heat. The efficiency of this process is often characterized in terms of a dimensionless figure of merit $ZT = GS^2T/\kappa$, where G is the electronic conductance, T is the average temperature, and κ is the thermal conductance. The thermopower S is defined as $S = -\Delta V/\Delta T$, where ΔV is the voltage difference between the two contacts of the molecular junction, resulting from a temperature difference ΔT. It is approximately given by $S = (\pi k_B)^2 T/(3e)\ [\mathrm{d}(\ln(\tau(E)))/\mathrm{d}E]_{E=E_F}$, where $\tau(E)$ now denotes the transmission function, k_B is the Boltzmann constant and e is the electron charge. In recent literature, several experimental studies on thermopower in molecular devices have been presented, both for the case of single molecular junctions and SAMs.[82–90] Since S is proportional to the slope of $\ln(\tau(E))$, specifically large thermopower values can be expected for molecular devices featuring a transmission node near the Fermi level.[91–93] Moreover, an ideal transmission function for a thermoelectric device would feature a transmission node close to a transmission peak, to ensure high values for both the conductance $G = 2e^2/h \cdot \tau(E)$ and the slope of $\ln(\tau(E))$ at $E = E_F$.[94] A clear example of tuning these is the cross-conjugated TDA system shown in Fig. 6(d), with its transmission minimum in the near vicinity of the HOMO transmission peak. For this molecule, our calculations yield a thermopower $S = 200\ \mu V\ K^{-1}$ which is much higher than typical values measured for conjugated molecular junctions ($<30\ \mu V\ K^{-1}$).

For true applications, junction stability will clearly be a serious issue. Devices based on SAMs are hence to be preferred (note that S does not depend on the number of molecules in parallel). Independent of future applicability, performing thermopower measurements on (cross-)conjugated molecules is exciting from a scientific point of view. First, because the sign of the slope of $\tau(E)$ distinguishes electron-like from hole-like transport. Second, because the magnitude of S can give independent evidence for QI features in cross-conjugated molecular junctions.

Conclusions and outlook

This perspective article has focused on two complementary topics in the field of molecular charge transport. The main goal has been to investigate the relationship between π-conjugation patterns, conductance, and quantum interference, thus connecting key concepts in (organic) chemistry and (quantum transport) physics. The secondary target has been to assess experimental robustness for two well-defined series of molecules, synthesized in one lab, by comparing conductance data obtained using different methods by different research groups. For that, we first studied a benchmark series of OPE wires. Conducting probe AFM data are found to be consistent with results from STM and MCBJ measurements on these same compounds. All data sets phenomenologically show exponential decay of conductance with length, characterized by a decay parameter β. More precisely, for CP-AFM, we find $\beta = 0.37 \pm 0.03\ Å^{-1}$, which is consistent with the values of 0.33 ± 0.02 and $0.34 \pm 0.01\ Å^{-1}$ found in STM and MCBJ measurements, respectively.[52] Interestingly, transport calculations match these data reasonably well, provided we do use the DFT + Σ method (giving $\beta_{DFT+\Sigma} = 0.31\ Å^{-1}$) instead of standard DFT (yielding $\beta_{DFT} = 0.16\ Å^{-1}$).

To study the role of quantum interference effects, we compare transport through three molecular wires with identical length, but different core units. We experimentally find the conductance of the cross-conjugated wire to be about two orders of magnitude lower than that of the linearly conjugated wire. Moreover, the conductance of the cross-conjugated wire is also lower than that of the molecular wire with broken conjugation. Again, this trend is confirmed by single-molecule measurements using the MCBJ method,[40,52] and by EGaIn junctions (with billions of molecules in parallel).[39] We present calculations demonstrating that these very low conductance values can be attributed to destructive quantum interference effects in cross-conjugated molecular wires.[38] Moreover, we show that this feature is quite general in cross-conjugated compounds. To provide an outlook to future experiments and possible devices, we also demonstrate theoretically that the energetic position of the quantum interference minimum in cross-conjugated compounds can be tuned by using different electron-rich or -poor side groups. This knowledge allows the design of cross-conjugated molecular wires for different purposes, for instance in thermoelectric devices.[94] Furthermore, the difference in conductance between cross-conjugated and linearly conjugated pathways through a molecule provides a basis for redox-active molecular switches, as well as for so-called π-logic.[95] In the latter concept, omniconjugated molecules[96] can be used to design electrical logic gates or to wire different molecular components.[97] To fully explore the opportunities that quantum interference effects offer in both fundamental and device-driven research,[98] it will be crucial to appreciate the relationship between quantum interference (a mainly physical concept) and cross-conjugation (more familiar to chemists).

Acknowledgements

We thank Dr Ryan Chiechi and prof. Thomas Wandlowski for the fruitful collaborations. We thank Petra Buiter and Jelmer Otten for their assistance with the synthesis of molecules AH-B and AC-B respectively. We thank Dr Eek Huisman for lively discussions. Prof. Petra Rudolf is acknowledged for the access to the XPS. We thank Dr Federica Galli for technical assistance. This work was supported by NanoNed (HV), funded by the Dutch Ministry of Economic Affairs (project GMM.6973), a VIDI grant (SJvdM), funded by the Netherlands Organization for Scientific Research (NWO), and the Danish Council for Independent Research Sapere Aude Program (KST) grant no. 11-1051390.

References

1 N. F. Phelan and M. Orchin, *J. Chem. Educ.*, 1968, **45**, 633.
2 C. A. van Walree, V. E. M. Kaats-Richters, S. J. Veen, B. Wieczorek, J. H. van der Wiel and B. C. van der Wiel, *Eur. J. Org. Chem.*, 2004, 3046–3056.
3 M. Gholami and R. R. Tykwinski, *Chem. Rev.*, 2006, **106**, 4997–5027.

4 D. Q. Andrews, G. C. Solomon, R. H. Goldsmith, T. Hansen, M. R. Wasielewski, R. P. Van Duyne and M. A. Ratner, *J. Phys. Chem. C*, 2008, **112**, 16991–16998.
5 A. B. Ricks, G. C. Solomon, M. T. Colvin, A. M. Scott, K. Chen, M. A. Ratner and M. R. Wasielewski, *J. Am. Chem. Soc.*, 2010, **132**, 15427–15434.
6 S. V. Aradhya and L. Venkataraman, *Nat. Nanotechnol.*, 2013, **8**, 399–410.
7 R. Baer and D. Neuhauser, *J. Am. Chem. Soc.*, 2002, **124**, 4200–4201.
8 G. C. Solomon, D. Q. Andrews, T. Hansen, R. H. Goldsmith, M. R. Wasielewski, R. P. Van Duyne and M. A. Ratner, *J. Chem. Phys.*, 2008, **129**, 054701.
9 G. C. Solomon, D. Q. Andrews, R. H. Goldsmith, T. Hansen, M. R. Wasielewski, R. P. Van Duyne and M. A. Ratner, *J. Am. Chem. Soc.*, 2008, **130**, 17301–17308.
10 T. Markussen, R. Stadler and K. S. Thygesen, *Nano Lett.*, 2010, **10**, 4260–4265.
11 C. Patoux, C. Coudret, J.-P. Launay, C. Joachim and A. Gourdon, *Inorg. Chem.*, 1997, **36**, 5037–5049.
12 S. Ballmann, R. Härtle, P. B. Coto, M. Elbing, M. Mayor, M. R. Bryce, M. Thoss and H. B. Weber, *Phys. Rev. Lett.*, 2012, **109**, 056801.
13 H. Vazquez, R. Skouta, S. Schneebeli, M. Kamenetska, R. Breslow, L. Venkataraman and M. S. Hybertsen, *Nat. Nanotechnol.*, 2012, **7**, 663–667.
14 A. E. Miroshnichenko, S. Flach and Y. S. Kivshar, *Rev. Mod. Phys.*, 2010, **82**, 2257–2298.
15 T. Markussen, J. Schiötz and K. S. Thygesen, *J. Chem. Phys.*, 2010, **132**, 224104.
16 R. Stadler, M. Forshaw and C. Joachim, *Nanotechnology*, 2003, **14**, 138–142.
17 D. M. Cardamone, C. A. Stafford and S. Mazumdar, *Nano Lett.*, 2006, **6**, 2422–2426.
18 C. A. Stafford, D. M. Cardamone and S. Mazumdar, *Nanotechnology*, 2007, **18**, 424014.
19 S.-H. Ke, W. Yang and H. U. Baranger, *Nano Lett.*, 2008, **8**, 3257–3261.
20 D. Q. Andrews, G. C. Solomon, R. P. Van Duyne and M. A. Ratner, *J. Am. Chem. Soc.*, 2008, **130**, 17309–17319.
21 N. Renaud, M. Ito, W. Shangguan, M. Saeys, M. Hliwa and C. Joachim, *Chem. Phys. Lett.*, 2009, **472**, 74–79.
22 M. Mayor, H. B. Weber, J. Reichert, M. Elbing, C. von Hänisch, D. Beckmann and M. Fischer, *Angew. Chem., Int. Ed.*, 2003, **42**, 5834–5838.
23 M. Kiguchi, H. Nakamura, Y. Takahashi, T. Takahashi and T. Ohto, *J. Phys. Chem. C*, 2010, **114**, 22254–22261.
24 J. R. Quinn, F. W. Foss, L. Venkataraman, M. S. Hybertsen and R. Breslow, *J. Am. Chem. Soc.*, 2007, **129**, 6714–6715.
25 M. Taniguchi, M. Tsutsui, R. Mogi, T. Sugawara, Y. Tsuji, K. Yoshizawa and T. Kawai, *J. Am. Chem. Soc.*, 2011, **133**, 11426–11429.
26 S. V. Aradhya, J. S. Meisner, M. Krikorian, S. Ahn, R. Parameswaran, M. L. Steigerwald, C. Nuckolls and L. Venkataraman, *Nano Lett.*, 2012, **12**, 1643–1647.
27 C. R. Arroyo, S. Tarkuc, R. Frisenda, J. S. Seldenthuis, C. H. M. Woerde, R. Eelkema, F. C. Grozema and H. S. J. van der Zant, *Angew. Chem., Int. Ed.*, 2013, **52**, 3152–3155.
28 S. N. Yaliraki and M. A. Ratner, *Ann. N. Y. Acad. Sci.*, 2002, **960**, 153–162.
29 S. J. van der Molen and P. Liljeroth, *J Phys.: Condens. Matter*, 2010, **22**, 133001.
30 M. Irie, *Chem. Rev.*, 2000, **100**, 1685–1716.
31 D. Dulic, S. J. van der Molen, T. Kudernac, H. T. Jonkman, J. J. D. de Jong, T. N. Bowden, J. van Esch, B. L. Feringa and B. J. van Wees, *Phys. Rev. Lett.*, 2003, **91**, 207402.
32 J. He, F. Chen, P. A. Liddell, J. Andréasson, S. D. Straight, D. Gust, T. A. Moore, A. L. Moore, J. Li, O. F. Sankey and S. M. Lindsay, *Nanotechnology*, 2005, **16**, 695–702.
33 S. J. van der Molen, H. van der Vegte, T. Kudernac, I. Amin, B. L. Feringa and B. J. van Wees, *Nanotechnology*, 2006, **17**, 310–314.
34 N. Katsonis, T. Kudernac, M. Walko, S. J. van der Molen, B. J. van Wees and B. L. Feringa, *Adv. Mater.*, 2006, **18**, 1397–1400.
35 A. J. Kronemeijer, H. B. Akkerman, T. Kudernac, B. J. Wees, B. L. Feringa, P. W. M. Blom and B. de Boer, *Adv. Mater.*, 2008, **20**, 1467–1473.
36 K. Matsuda, H. Yamaguchi, T. Sakano, M. Ikeda, N. Tanifuji and M. Irie, *J. Phys. Chem. C*, 2008, **112**, 17005–17010.
37 S. J. van der Molen, J. Liao, T. Kudernac, J. S. Agustsson, L. Bernard, M. Calame, B. J. van Wees, B. L. Feringa and C. Schönenberger, *Nano Lett.*, 2009, **9**, 76–80.
38 C. M. Guédon, H. Valkenier, T. Markussen, K. S. Thygesen, J. C. Hummelen and S. J. van der Molen, *Nat. Nanotechnol.*, 2012, **7**, 305–309.
39 D. Fracasso, H. Valkenier, J. C. Hummelen, G. C. Solomon and R. C. Chiechi, *J. Am. Chem. Soc.*, 2011, **133**, 9556–9563.
40 W. Hong, H. Valkenier, G. Mészáros, D. Z. Manrique, A. Mishchenko, A. Putz, P. M. García, C. J. Lambert, J. C. Hummelen and T. Wandlowski, *Beilstein J. Nanotechnol.*, 2011, **2**, 699–713.
41 E. H. van Dijk, D. J. T. Myles, M. H. van der Veen and J. C. Hummelen, *Org. Lett.*, 2006, **8**, 2333–2336.
42 G. Chen and Y. Zhao, *Tetrahedron Lett.*, 2006, **47**, 5069–5073.
43 J. K. Sørensen, M. Vestergaard, A. Kadziola, K. Kilså and M. B. Nielsen, *Org. Lett.*, 2006, **8**, 1173–1176.
44 M. Vestergaard, K. Jennum, J. K. Sørensen, K. Kilså and M. B. Nielsen, *J. Org. Chem.*, 2008, **73**, 3175–3183.
45 S. Tsoi, I. Griva, S. A. Trammell, A. S. Blum, J. M. Schnur and N. Lebedev, *ACS Nano*, 2008, **2**, 1289–1295.
46 S. Tsoi, I. Griva, S. A. Trammell, G. Kedziora, J. M. Schnur and N. Lebedev, *Nanotechnology*, 2010, **21**, 085704.
47 N. Darwish, I. Díez-Pérez, P. Da Silva, N. Tao, J. J. Gooding and M. N. Paddon-Row, *Angew. Chem., Int. Ed.*, 2012, **51**, 3203–3206.
48 V. Rabache, J. Chaste, P. Petit, M. L. Della Rocca, P. Martin, J.-C. Lacroix, R. L. McCreery and P. Lafarge, *J. Am. Chem. Soc.*, 2013, **135**, 10218–10221.
49 H. Valkenier, E. H. Huisman, P. A. van Hal, D. M. de Leeuw, R. C. Chiechi and J. C. Hummelen, *J. Am. Chem. Soc.*, 2011, **133**, 4930–4939.

50 D. J. Wold and C. D. Frisbie, *J. Am. Chem. Soc.*, 2001, **123**, 5549–5556.
51 J. M. Tour, L. R. Jones II, D. L. Pearson, J. J. S. Lamba, T. P. Burgin, G. M. Whitesides, D. L. Allara, A. N. Parikh and S. V. Atre, *J. Am. Chem. Soc.*, 1995, **117**, 9529–9534.
52 V. Kaliginedi, P. Moreno-García, H. Valkenier, W. Hong, V. M. García-Suárez, P. Buiter, J. L. H. Otten, J. C. Hummelen, C. J. Lambert and T. Wandlowski, *J. Am. Chem. Soc.*, 2012, **134**, 5262–5275.
53 The distance from sulfur to sulfur atom.
54 J. Yang, A. Dass, A.-M. M. Rawashdeh, C. Sotiriou-Leventis, M. J. Panzner, D. S. Tyson, J. D. Kinder and N. Leventis, *Chem. Mater.*, 2004, **16**, 3457–3468.
55 T. R. Criswell and B. H. Klanderman, *J. Org. Chem.*, 1974, **39**, 770–774.
56 P. Hodge, G. A. Power and M. A. Rabjohns, *Chem. Commun.*, 1997, 73–74.
57 S.-K. Kwon, Y.-H. Kim, J.-W. Park, D. M. Kang, S. O. Jung, J. Y. Baek, M.-H. Park, J. U. Ju, T. H. Kim, S. H. Jang, S.-G. Lee, S. J. Park, J.-S. Kim and J.-K. Park, *WO Pat.*, 120839, 2008.
58 R. N. Renaud and J. C. Stephens, *Can. J. Chem.*, 1974, **52**, 1229–1230.
59 F. Keller and C. Rüchardt, *J. Prakt. Chem./Chem.-Ztg.*, 1998, **340**, 642–648.
60 R. Chinchilla and C. Nájera, *Chem. Rev.*, 2007, **107**, 874–944.
61 N. Stuhr-Hansen, J. K. Sørensen, K. Moth-Poulsen, J. B. Christensen, T. Bjørnholm and M. B. Nielsen, *Tetrahedron*, 2005, **61**, 12288–12295.
62 A. Blaszczyk, M. Elbing and M. Mayor, *Org. Biomol. Chem.*, 2004, **2**, 2722–2724.
63 Our attempts to cross-couple 2,6-dibromo-9,10-anthraquinone directly with 1-ethynyl-4-thioacetylbenzene were not successful.
64 N. N. P. Moonen, W. C. Pomerantz, R. Gist, C. Boudon, J.-P. Gisselbrecht, T. Kawai, A. Kishioka, M. Gross, M. Irie and F. Diederich, *Chem.–Eur. J.*, 2005, **11**, 3325–3341.
65 A more detailed spectroscopic study on similar anthraquinone-based wires with various electron donating and withdrawing groups is presented in ref. 54.
66 V. B. Engelkes, J. M. Beebe and C. D. Frisbie, *J. Phys. Chem. B*, 2005, **109**, 16801–16810.
67 A. Salomon, D. Cahen, S. Lindsay, J. Tomfohr, V. B. Engelkes and C. D. Frisbie, *Adv. Mater.*, 2003, **15**, 1881–1890.
68 A. J. Kronemeijer, E. H. Huisman, I. Katsouras, P. A. van Hal, T. C. T. Geuns, P. W. M. Blom, S. J. van der Molen and D. M. de Leeuw, *Phys. Rev. Lett.*, 2010, **105**, 156604.
69 A. J. Kronemeijer, PhD thesis, University of Groningen, 2011, (*online available at*: http://irs.ub.rug.nl/ppn/333711378).
70 K. Liu, G. Li, X. Wang and F. Wang, *J. Phys. Chem. C*, 2008, **112**, 4342–4349.
71 Y. Xing, T.-H. Park, R. Venkatramani, S. Keinan, D. N. Beratan, M. J. Therien and E. Borguet, *J. Am. Chem. Soc.*, 2010, **132**, 7946–7956.
72 Q. Lu, K. Liu, H. Zhang, Z. Du, X. Wang and F. Wang, *ACS Nano*, 2009, **3**, 3861–3868.
73 W. Hong, H. Li, S.-X. Liu, Y. Fu, J. Li, V. Kaliginedi, S. Decurtins and T. Wandlowski, *J. Am. Chem. Soc.*, 2012, **134**, 19425–19431.
74 S. Creager, C. J. Yu, C. Bamdad, S. O'Connor, T. MacLean, E. Lam, Y. Chong, G. T. Olsen, J. Luo, M. Gozin and J. F. Kayyem, *J. Am. Chem. Soc.*, 1999, **121**, 1059–1064.
75 See the ESI† for the standard DFT transmission functions.
76 D. J. Mowbray, G. Jones and K. S. Thygesen, *J. Chem. Phys.*, 2008, **128**, 111103.
77 S. Y. Quek, H. J. Choi, S. G. Louie and J. B. Neaton, *Nano Lett.*, 2009, **9**, 3949–3953.
78 J. B. Neaton, M. S. Hybertsen and S. G. Louie, *Phys. Rev. Lett.*, 2006, **97**, 216405.
79 M. L. Perrin, C. J. O. Verzijl, C. A. Martin, A. J. Shaikh, R. Eelkema, J. H. van Esch, J. M. van Ruitenbeek, J. M. Thijssen, H. S. J. van der Zant and D. Dulić, *Nat. Nanotechnol.*, 2013, **8**, 282–287.
80 R. Härtle, M. Butzin, O. Rubio-Pons and M. Thoss, *Phys. Rev. Lett.*, 2011, **107**, 046802.
81 T. Markussen, R. Stadler and K. S. Thygesen, *Phys. Chem. Chem. Phys.*, 2011, **13**, 14311–14317.
82 P. Reddy, S. Y. Jang, R. A. Segalman and A. Majumdar, *Science*, 2007, **315**, 1568–1571.
83 K. Baheti, J. A. Malen, P. Doak, P. Reddy, S. Y. Jang, T. D. Tilley, A. Majumdar and R. A. Segalman, *Nano Lett.*, 2008, **8**, 715–719.
84 J. A. Malen, P. Doak, K. Baheti, T. D. Tilley, R. A. Segalman and A. Majumdar, *Nano Lett.*, 2009, **9**, 1164–1169.
85 A. Tan, S. Sadat and P. Reddy, *Appl. Phys. Lett.*, 2010, **96**, 013110Q2.
86 S. K. Yee, J. A. Malen, A. Majumdar and R. A. Segalman, *Nano Lett.*, 2011, **11**, 4089–4094.
87 A. Tan, J. Balachandran, S. Sadat, V. Gavini, B. D. Dunietz, S. Y. Jang and P. Reddy, *J. Am. Chem. Soc.*, 2011, **133**, 8838–8841.
88 J. R. Widawsky, P. Darancet, J. B. Neaton and L. Venkataraman, *Nano Lett.*, 2011, **12**, 354–358.
89 C. Evangeli, K. Gillemot, E. Leary, M. T. Gonzalez, G. Rubio-Bollinger, C. J. Lambert and N. Agraït, *Nano Lett.*, 2013, **13**, 2141–2145.
90 D. Nozaki, H. Sevinçli, W. Li, R. Gutiérrez and G. Cuniberti, *Phys. Rev. B: Condens. Matter Mater. Phys.*, 2010, **81**, 235406.
91 J. P. Bergfield and C. A. Stafford, *Nano Lett.*, 2009, **9**, 3072–3076.
92 C. M. Finch, V. M. Garcia-Suarez and C. J. Lambert, *Phys. Rev. B: Condens. Matter Mater. Phys.*, 2009, **79**, 033405.
93 J. P. Bergfield, M. A. Solis and C. A. Stafford, *ACS Nano*, 2010, **4**, 5314–5320.
94 R. Stadler and T. Markussen, *J. Chem. Phys.*, 2011, **135**, 154109.
95 M. H. van der Veen, PhD thesis, University of Groningen, 2006, (*online available at*: http://irs.ub.rug.nl/ppn/293902518).
96 M. H. van der Veen, M. T. Rispens, H. T. Jonkman and J. C. Hummelen, *Adv. Funct. Mater.*, 2004, **14**, 215–223.
97 E. Lörtscher, *Nat. Nanotechnol.*, 2013, **8**, 381–384.
98 S. J. van der Molen, R. Naaman, E. Scheer, J. B. Neaton, A. Nitzan, D. Natelson, N. J. Tao, H. S. J. van der Zant, M. Mayor, M. Ruben, M. Reed and M. Calame, *Nat. Nanotechnol.*, 2013, **8**, 385–389.

